PERGAMON

Engineering Failure Analysis 9 (2002) 167–184

ENGINEERING FAILURE ANALYSIS

Characteristics of hydrogen embrittlement, stress corrosion cracking and tempered martensite embrittlement in high-strength steels

N. Eliaz [a,*,1], A. Shachar [b,c], B. Tal [b], D. Eliezer [c]

[a] *H.H. Uhlig Corrosion Laboratory, Massachusetts Institute of Technology, Cambridge, MA 02139-4307, USA*
[b] *Metallurgical Laboratory, Israel Air Force, PO Box 02745, Israel*
[c] *Department of Materials Engineering, Ben-Gurion University, PO Box 653, Beer-Sheva 84105, Israel*

Received 23 November 2000; accepted 26 December 2000

Abstract

Characteristics of tempered martensite embrittlement (TME), hydrogen embrittlement (HE), and stress corrosion cracking (SCC) in high-strength steels are reviewed. Often, it is important to determine unambiguously by which of these mechanisms failure occurred, in order to suggest the right actions to prevent failure recurrence. To this aim, samples made of high-strength AISI 4340 alloy steel were embrittled by controlled processes that might take place, for example, during the fabrication and service of aircraft landing gears. The samples were then fractured and characterized using light and scanning electron microscopy, microhardness tests, and X-ray diffraction. Fractography was found to be the most useful tool in determining which of these mechanisms is responsible for a failure, under similar conditions, of structures made of AISI 4340 alloy steel.

Keywords: Failure analysis; Hydrogen embrittlement; Stress-corrosion cracking; Structural steel; Tempered martensite embrittlement

1. Introduction

An essential step in failure analysis is the determination of the failure mechanism. Identifying whether failure has occurred by, for example, overload, metallurgical embrittlement, or environment-assisted cracking, allows the determination of the underlying cause of failure and recommendation on proper actions to prevent failure recurrence. In this context, environment-assisted cracking (EAC), or environmentally induced cracking (EIC), is a form of corrosion that produces a brittle fracture in alloys with minimal uniform corrosion [1]. This general term encompasses more specific processes such as stress corrosion cracking

* Corresponding author. Present address: Department of Solid Mechanics, Materials and Systems, Tel Aviv University, Tel Aviv 69978, Israel. Tel.: +972-3-640-7384; fax: +972-3-640-7617.
E-mail address: neliaz@eng.tan.ac.il (N. Eliaz).

[1] Formerly with the Metallurgical Laboratory of the Israel Air Force and the Department of Materials Engineering at Ben-Gurion University.

1350-6307/02/$ - see front matter
PII: S1350-6307(01)00009-7

(SCC), corrosion fatigue cracking (CFC), and hydrogen-induced cracking (HIC). The latter is also referred to as hydrogen embrittlement (HE), or hydrogen-assisted cracking (HAC).

Unfortunately, for high-strength steels, distinguishing between failure mechanisms is often difficult because similar fracture characteristics (namely, brittle intergranular fracture along prior-austenite grain-boundaries) can occur for a variety of reasons [2]. For example, in several failure analyses that were conducted in the Metallurgical Laboratory of the Israel Air Force, it was difficult to determine whether failures of landing gears made of high-strength AISI 4340 alloy steel occurred as a result of TME (tempered martensite embrittlement), SCC, or HE. The fabrication of these landing gears typically involves quenching and tempering heat treatment to obtain high strength, as well as electrodeposition of hard chromium. During service, however, these parts are also exposed to conditions which favor SCC. Therefore, a project was initiated in which samples made of this steel were embrittled by controlled processes, fractured, and characterized using some common laboratory techniques. The controlled processes were selected as to best simulate events that might occur during the fabrication and service of landing gears. Thus, the objective of this work was twofold: (1) to determine the usefulness of different characterization techniques in distinguishing between TME, SCC and HE; and (2) to establish a database that could be used as a reference for future failure analyses of components made of the same steel.

In the framework of the first stage of the project, to be presented in this paper, there was no use of techniques such as secondary ion mass spectrometry (SIMS), atomic force microscopy (AFM), and computer modelling. It should be noted, however, that these techniques can provide valuable data in determining the mechanisms of failures. Before presenting the authors' experimental work, let us review the major characteristics of TME, HE and SCC in high-strength steels.

1.1. Tempered martensite embrittlement

Improper heat treatment of steels might lead to one of two forms of embrittlement. The first form results from a two-step heat treatment, which includes heavy tempering at a temperature above 600°C, and aging within (or slow cooling through) the temperature range of 350–600°C. In this case, the embrittlement is manifested by increased ductile-to-brittle transition temperature, and is referred to as temper embrittlement. The second form of embrittlement, and the one of interest in this work, results from a one-step tempering of high-strength martensitic (or lower-bainitic) steels at temperatures within the range of 250–400°C. In this case, the embrittlement is manifested by reduced room-temperature notched-bar impact energy, or as reduced tensile properties of unnotched samples tested at subzero temperatures. This form of embrittlement is known as tempered martensite embrittlement (TME) [3–5].

TME is related to intergranular embrittlement caused by the combination of impurity (e.g. P, S, N, Sb and Sn) segregation to grain-boundaries during austenitization, and cementite (Fe_3C) precipitation along prior-austenite grain-boundaries during tempering. The extent of impurity segregation, and thus of embrittlement, is enhanced by the presence of Mn and Si in the alloy. The extent of embrittlement also depends on the austenitization temperature, as will be shown in Section 3. As the austenitization temperature is raised, the grain size increases, and thus the area of grain-boundaries decreases. Consequently, the grain-boundaries become more enriched with impurities, and the embrittlement phenomenon is more pronounced.

The effect of tempering temperature on the susceptibility to TME can be explained in the following way. At temperatures lower than 250°C, the amount of carbides that precipitate at grain-boundaries is insufficient to cause embrittlement. Above approximately 400°C, however, the carbides become spheroidal and occupy a smaller fraction of the grain-boundary area. Consequently, the steel softens and its toughness increases. In general, the dependence of embrittlement occurrence on carbide precipitation is related to the retarding effect of these carbides on dislocation motion, thus enhancing formation of dislocation pileups at (already weakened) grain-boundaries. Such dislocation pileups would lead to initiation of intergranular (IG) fracture much before yielding can take place in the neighbor grains [4].

Except of preparing high-purity (but expensive) alloys, the best way to prevent TME is to avoid tempering within the dangerous temperature range. Usually, this involves tempering at a higher temperature, but with some compromise on strength. However, when applications require higher strengths associated with tempering at 300°C, it is still possible to suppress the kinetics of TME by adding 1.5–2% Si to the steel [5].

1.2. Hydrogen embrittlement

Under certain conditions, hydrogen can degrade the fracture behavior of most structural alloys. Embrittlement can occur as a result of hydrogen located within the bulk of the alloy during the application of a load (''internal hydrogen embrittlement''). In addition, embrittlement might result from the exposure of an alloy under load to a hydrogen-containing environment (''external hydrogen embrittlement''). The embrittlement is manifested by the non-ductile fracture mode, reduced ductility, and reduced tensile strength [6].

The HE process depends on three major factors: (1) the origin of the hydrogen; (2) the transport processes involved in moving the hydrogen from its source to the locations where it reacts with the metal to cause embrittlement; and (3) the embrittling mechanism itself. Several embrittling mechanisms have been proposed for crystalline materials (see, for example [6–11] and references therein). The most common HE mechanisms are the high-pressure bubble formation, reduction in surface energy (adsorption mechanism), reduction in the lattice cohesive force (decohesion mechanism), hydrogen interaction with dislocations, and hydride formation.

In high-strength steels (yield strength greater than 170 ksi), the effect of internal hydrogen supersaturation is significant. Internal HE by the mechanism of high-pressure bubble formation might be extremely severe due to the ease of cavity (microcrack) growth. Degradation is most severe under static loads or at low strain rates, where high internal hydrogen pressures can be maintained within the cavity or microcrack. Since hydrogen interacts with the high-strength martensitic structure, fractographic evidence of hydrogen degradation by internal pressure formation often exists. Isolated areas are observed of either IG or TG (transgranular) fracture by brittle cleavage or interface separation, depending on the relative strength of the grain-boundaries. These areas are separated by other areas exhibiting the normal fracture mode for rapid, overload failure in the alloy (e.g. microvoid coalescence or quasicleavage) [6]. In principal, the presence of hydrogen may also lead to the appearance of 'hairlines' on the facets of some grains, or to a change in the size of microvoids.

Hydrogen need not be present in concentrations above the solid-solution solubility limit to embrittle martensitic and ferritic steels. Both structures can be strongly degraded by relatively low concentrations of hydrogen originating either from the bulk of the alloy or from a hydrogen-containing environment. In general, the higher the strength level of the steel, the greater its susceptibility to HE. At low concentration of hydrogen, the exact mechanism of embrittlement is often difficult to establish. The fracture surfaces of smooth and notched tensile specimens often exhibit a brittle-to-ductile transition failure. At the region in contact with hydrogen, fracture is generally IG, occurring by interface separation of the grain-boundaries. At the other regions of the specimen, failure represents the virgin material and may be of a ductile mode [6].

Nowadays, there is an increasing demand for lighter and higher strength steels. This demand results from the need to improve the performance of structures such as aircraft landing gears and arresting hooks, defense and offshore platforms, bridges, military armor, first walls and blankets in fusion reactors, etc. Some of these advanced steels (e.g. AerMet 100) use new concepts of strengthening, for instance precipitation, and not just the traditional eutectoidal decomposition. In addition to strength and weight requirements, advanced ultra-high-strength steels must meet stringent requirements with respect to fracture toughness and resistance to EAC. With the use of steels of ever-increasing strength level, hydrogen distribution in the steel is becoming a more serious issue. As the strength level increases, the amount of allowable diffusible hydrogen content decreases, sometimes to the level of uncertainty in the practice of diffusible hydrogen measurements. At these lower hydrogen levels, the hydrogen distribution is as important as the average diffusible hydrogen

content. For higher-strength steels, the importance of the local concentration of hydrogen, rather than its average total content, has been demonstrated in several studies. For example, embrittlement of high-chromium martensitic steels for nuclear reactors was observed for relatively low average hydrogen content (a few ppm) and within a rather large temperature range (from −130 to 250°C) [12]. Consequently, there is a need for new approaches to improve hydrogen management in these steels. One possible approach is the use of specific hydrogen traps in steels in order to reduce and control the diffusible hydrogen level.

The effects of the chemical composition of the steel on hydrogen absorption and the steel susceptibility to HE have been discussed in numerous papers (e.g. [13–23]). In general, alloying elements and impurities may affect the interaction of the steel with hydrogen by changing the corrosion potential of the steel, poisoning surfaces such as grain-boundaries, forming precipitates and inclusions that act as traps, forming protective surface layers, etc. In addition to chemical composition, a great variety of metallurgical parameters can influence the susceptibility of a structural steel to hydrogen. These parameters include the kind, size, and distribution of different phases; the grain size of the steel; and the degree of cold work [5,6,12,24–27].

Although hydrogen diffusion in the martensitic and ferritic structures is relatively rapid, it is not always a simple task to remove this hydrogen once it has entered the steel. Baking at elevated temperatures is one practice commonly employed with some degree of success. Although hydrogen diffusion is exponentially increased with temperature, the required time to reduce the hydrogen concentration to a given level increases with the square of the section thickness. For thick sections this can mean hundreds of hours at any common baking temperature. Even then, there is no guarantee that permanent damage or irreversible HE has not already occurred. Irreversible HE can simply be the nucleation and partial growth of cavities by the precipitation of hydrogen prior to its removal. As a result of the low fracture toughness of these steels and the inability to remove all hydrogen from the microcracks, time-dependent crack growth can occur in these steels even at low partial pressures of hydrogen [6].

1.3. Stress corrosion cracking

SCC is a phenomenon associated with the combination of static tensile stress and corrosive environment. Failures often occur in mild environments under tensile stresses well below the macroscopic yield strength of the material. The origin of tensile stresses may be external forces, thermal stresses, or residual stresses. In general, as these stresses increase, the time required to initiate SCC decreases. The kinetics of SCC also depends on the chemical and metallurgical state of the material (i.e. chemical composition, thermal condition, grain size, presence of secondary phases and precipitates, etc.); on environmental conditions (e.g. environment composition, temperature, pressure, pH, electrochemical potential, solution viscosity and mixing, etc.); and on crack geometry and stress state (i.e. uniaxial, triaxial, etc.) [1,5,28].

SCC may be either IG or TG, depending on the alloy, its microstructure, and the environment. However, the crack follows a general macroscopic path that is always normal to the tensile component of stress. TG failures are less common than the IG ones, but both may exist in the same system or even in the same failed part, depending on conditions. The IG failure mode suggests some inhomogeneity at the grain-boundaries. For example, segregation of S and P at grain-boundaries has been suggested as the cause of IG SCC of low alloy steels [1].

Numerous mechanisms have been proposed for SCC [1,5,28–30]. Among these mechanisms are the hydrogen embrittlement, adsorption-induced cleavage, atomic surface mobility, film rupture, stress-accelerated dissolution, film-induced cleavage, tunnel pitting and tearing, and localized surface plasticity mechanisms. There has been some evidence, for example, that the solution within the microvolume of the crack becomes acidified, probably by hydrolysis reactions similar to those which occur in pits. Therefore, the presence of hydrogen in the crack and the brittle cleavage characteristics of TG cracks have prompted support for the HE mechanism, at least for certain high-strength materials.

1.4. Comparison between hydrogen embrittlement and stress corrosion cracking

It is difficult to make unequivocal statements regarding the characteristics of any of the forms of EAC because exceptions are not unusual. Nevertheless, Table 1 [1] compares between the common characteristics of HE and SCC. The data in this table should be regarded only as general guidelines.

HE and SCC may be distinguished from each other by consideration of the background information; the extent, nature, and distribution of corrosion; the sites of crack initiation; and other factors. Factors which favor SCC as a failure mechanism include: (1) an in-service environment capable of producing SCC, and conversely, an absence of pre-treatments which could introduce hydrogen into the steel prior to service; (2) multiple cracks initiated from corrosion pits; and (3) corrosion products on the fracture surface, which become thicker closer to the origin. Factors which favor HE include: (1) inadequate baking following coating, or the use of other treatments that could introduce hydrogen into the steel; and (2) exposure of a component to low-humidity air in service [2].

Fractures produced by HE could become corroded after cracking, but such corrosion is generally manifested by patches of rust on both IG and dimpled overload areas rather than by the more uniform, often black, corrosion film found on SCC fractures. HE failures sometimes initiate from subsurface inclusions, but it is often not possible to distinguish between surface initiation sites and initiation sites at small inclusions close to the surface. Moreover, SCC often exhibits more crack branching and less pronounced, partially-formed, dimples than cracking produced by HE. However, the extent of crack branching and dimples also depends on the stress intensity at the crack tip, on hydrogen concentration or environment, and on the composition and thermal condition of the steel. Because some of this information is often not known for in-service failures, these features cannot be reliably used to distinguish between HE and SCC [2].

2. Experimental procedure

In general, the concept of this work was to prepare standard samples from the same batch of steel, to embrittle them in a controlled manner by different processes, to let the samples fracture, and then to characterize the fracture surfaces and the material just beneath them using light and scanning electron microscopy, microhardness testing, and X-ray diffraction. All specimens were fabricated from the same rod of AISI 4340 alloy steel. The raw material was examined and found to satisfy the requirements of AMS 6415 [31]. The chemical composition of this material is shown in Table 2.

The different samples and embrittling processes used in this work are summarized in Table 3. All heat treatments (austenitization, quenching, tempering, and air-cooling to obtain hardness within the range of

Table 1
Comparison between typical characteristics of hydrogen embrittlement (HE) and stress-corrosion cracking (SCC) [1]

Characteristic	SCC	HE
Stress	Static tensile	Static tensile
Aqueous corrosive environment	Specific to the alloy	Any
Temperature increase	Accelerates	Increases to RT, then decreases
Pure metal	More resistant	Susceptible
Crack morphology	TG or IG branched sharp tip	TG or IG unbranched sharp tip
Corrosion products in the crack	Absent (usually)	Absent (usually)
Crack surface appearance	Cleavage-like	Cleavage-like
Cathodic polarization	Suppresses (usually)	Accelerates
Strain-rate increase	Decreases	Decreases
Near maximum strength level	Susceptible, but HE often predominates	Accelerates

Table 2
The chemical composition (wt.%) of the studied AISI 4340 steel, as obtained by optic emission spectrometer. The requirements of the AMS 6415 standard are also shown for comparison

	C	Ni	Cr	Mn	Mo	Si	S	Fe
Steel studied	0.41	1.88	0.87	0.76	0.27	0.33	0.02	Rem.
AMS 6415	0.38-0.43	1.65-2.00	0.70-0.90	0.65-0.85	0.20-0.30	0.15-0.35	0.025 max	Rem.

Table 3
Samples and experimental procedures

Sample index	Sample type	Treatment	Loading
REF1	Tensile V-notch (43–46 R_C)	–	Impact to failure
REF2	Tensile V-notch (43–46 R_C)	–	Tensile test to failure
H1, H2	Tensile V-notch (43–46 R_C)	Hard chromium electroplating, no baking	Tension under constant load
H3, H4	Tensile V-notch (43–46 R_C)	Cadmium electroplating, no baking	Tension under constant load
H5, H6	Tensile V-notch (50–53 R_C)	Cadmium electroplating, no baking	Tension under constant load
SCC1	Tensile V-notch (43–46 R_C)	–	Simultaneous tension under constant load and exposure to 3.5% NaCl solution
SCC2, SCC3	C-ring (43–46 R_C)	Wax coating	Simultaneous constant-strain loading and alternate exposure to 3.5% NaCl solution
TME1	Tensile V-notch	Austenitization at 850°C, oil quenching, tempering at 350°C	Impact to failure
TME2	Tensile V-notch	Austenitization at 850°C, oil quenching, tempering at 350°C	Tensile test to failure
TME3	Tensile V-notch	Austenitization at 1000°C, oil quenching, tempering at 350°C	Impact to failure
TME4	Tensile V-notch	Austenitization at 1100°C, oil quenching, tempering at 350°C	Impact to failure
TME5	Tensile V-notch	Austenitization at 1100°C in vacuum (10^{-4} torr), oil quenching, tempering at 350°C	Impact to failure

either 43–46 or 50–53 R_C) followed the requirements of P.S. 01.9001 [32]. Standard tensile V-notch (TVN) samples were machined in accordance with the requirements of ASTM F 519 [33]. A typical TVN sample is shown in Fig. 1.

Hydrogen was introduced to some samples by electrodeposition. Hard chromium electrodeposition was carried out in accordance with the requirements of QQ-C-320 [34]. Because the cathode efficiency may have a significant effect on the amount of hydrogen absorbed in the coated metal, some samples were electrodeposited with cadmium (which has a much higher cathode efficiency compared to hard chromium), following the requirements of QQ-P-416 [35]. Normally, baking at a temperature within the range of 177–205°C for at least 3 h is required following electrodeposition of high-strength steels in order to prevent HE. This heat treatment is required for all steel parts hardened to at least 40 R_C, and should be applied not later than 4 h after the completion of the plating process [34]. However, because the aim of this work was, in part, to simulate possible improper manufacturing processes, no baking was done. The notched samples were tested under constant load, following the specifications in ASTM E 8 [36]. The standard requirement is that all samples sustain a load of 75% of the fracture load for at least 200 h without cracking [33].

For SCC testing, both standard TVN and standard C-ring samples were used. The TVN sample was tested using the same procedure as described above. However, the notch (and its vicinity) was simultaneously

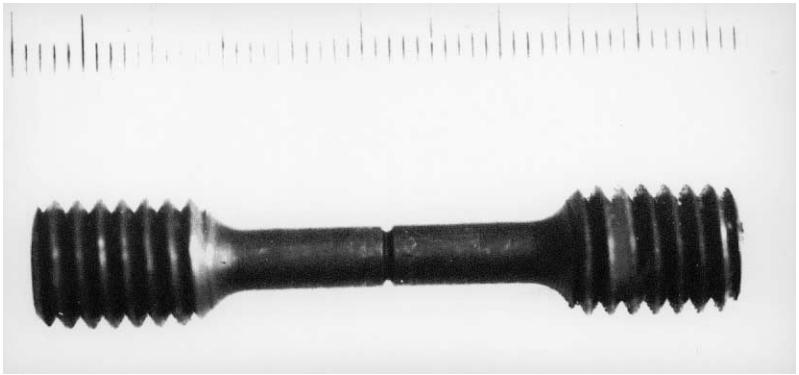

Fig. 1. Standard tensile V-notch sample.

exposed to a solution of 3.5% NaCl. C-ring samples were prepared following the requirements of ASTM G 38 [37]. An advantage of the C-ring is that it can be stressed with high precision and bias by application of a measured deflection. The basic C-ring is a constant-strain specimen with tensile stress produced on the exterior of the ring by tightening a bolt centered on the diameter of the ring. The stress of main interest in such a specimen is the circumferential stress, which varies from zero at each bolt hole to a maximum at the middle of the arc opposite the stressing bolt. The C-rings were stressed based on calculation of the deflection required to develop a stress of 75% of the ultimate tensile strength, setting the individual ring dimensions into the following modified curved beam equation [37]:

$$\mathrm{OD_f} = \mathrm{OD} - \delta \tag{1}$$

$$\delta = \sigma \pi D^2 / 4EtZ \tag{2}$$

where OD is the outer diameter of the C-ring before stressing (mm), $\mathrm{OD_f}$ the outer diameter of stressed C-ring (mm), σ the desired stress within the proportional limit (psi), δ the change in the outer diameter giving the desired stress (mm), $D = (OD - t)$ the mean diameter (mm), t the wall thickness (mm), E the modulus of elasticity (psi), and Z a correction factor for curved beams which depends on the D/t ratio.

After tightening, both the bolt and the C-ring, except the middle of the arc opposite the bolt, were wax-coated. The purpose of this coating was to prevent any galvanic coupling, as well as to 'force' failure to occur within a desired (uncoated) area. The samples were subsequently immersed in an aqueous solution of 3.5% NaCl, removed periodically, and inspected for visual evidence of stress corrosion cracks. The alternate immersion test utilized a 1-h cycle that included a 10-min period in the solution and a 50-min period out of the solution, in accordance with ASTM G 44 [38]. This 1-h cycle was continued until failure occurred.

TME was induced following different austenitization treatments (Table 3), using standard TVN samples. For some materials such as high-strength steels, overload fractures may look similar to other fracture modes. Hence, two TVN reference samples were loaded to failure by tension and by impact, respectively. This procedure allowed determination of the normal overload fracture surface appearance under different strain rates.

Following failure, all fracture surfaces were examined, using stereomicroscopy and scanning electron microscopy (SEM). Metallographic cross-sections were prepared perpendicular to the fracture surface. The macro- and microstructure were examined before and after chemical etching in Nital solution (3% HNO_3 in ethanol), respectively, using light microscopy (LM). In addition to supporting the determination of crack path, metallographic sections through origins can prove whether 'abnormal' features such as large inclusions, porosity, grain-boundary films, untempered martensite, or corrosion pits, facilitated crack initiation.

Microhardness scans were carried out from the fracture surface into the bulk of the material, at 0.1-mm intervals, applying a load of 500 g. Finally, thin slices were cut from the region just beneath the fracture surface. These slices were subsequently characterized using X-ray diffraction (XRD) under the following conditions: Co radiation ($\lambda = 1.79021$ Å), $V = 40$ kV, $I = 28$ mA, scanning from 45 to 135° at a scan rate of 1°/min.

3. Results and discussion

Fig. 2 shows the typical features of the fracture surface of sample REF1 (see Table 3). The fracture is characterized by a combination of overload microvoids and some IG regions. No abnormal features were observed in the metallographic cross-section of this sample, either before or after chemical etching. Fig. 3 shows the typical features of the fracture surface of sample REF2. In general, these features are similar to the ones reported for sample REF1 (although the fracture of sample REF1 appears to be more brittle). Thus, the presence of IG regions can be related to the high strength (hardness) of the material and to the presence of a notch, rather than to the high loading rate involved in an impact test.

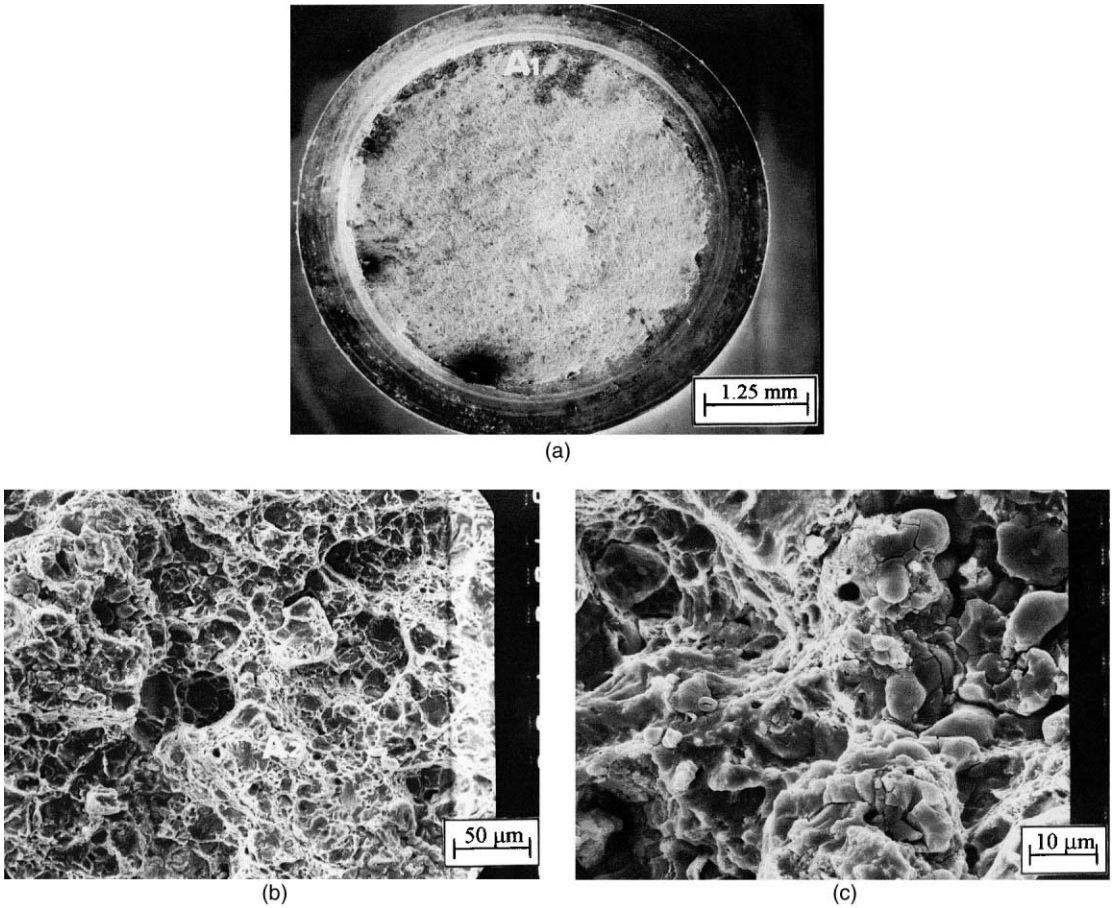

Fig. 2. SEM view of the fracture surface of a tensile V-notch sample made of AISI 4340 alloy steel (43–46 R_C) and fractured by impact. (b) Higher magnification of region A_1 in (a). Similarly, (c) is a higher magnification of region A_2 in (b).

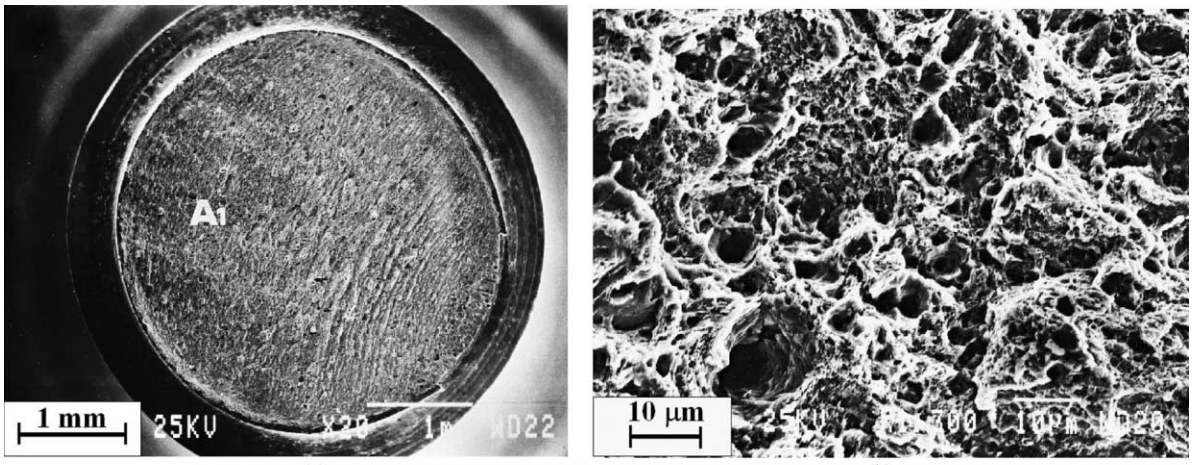

(a) (b)

Fig. 3. SEM view of the fracture surface of a tensile V-notch sample made of AISI 4340 alloy steel (43–46 R_C) and fractured by tension. (b) Higher magnification of region A_1 in (a).

In the absence of baking, samples H1 and H2 failed within few seconds of loading. The fracture surface of these samples (Fig. 4) was composed of an inner microvoid (overload) TG region, and a peripheral IG region. The IG path along prior-austenite grain-boundaries is typical of failures of high-strength steels in HE mechanism, as discussed in Section 1. From Fig. 4(a) it is evident that some secondary cracking exists in these samples. Fig. 4(b) shows that the region around this secondary cracking is completely IG. Fig. 4(c) shows that some grain facets are not flat, but rather dimpled. This feature may be related to the presence of discrete globular phases in the steel, as well as to local effects of hydrogen. Metallography showed no abnormal features in these samples.

Contrary to the results for the chromium-coated steel, samples H3 and H4 (which were cadmium-coated) were able to sustain a load of 75% of the fracture load for 200 h without being cracked. Fig. 5 shows a typical fracture surface of these samples, after they eventually fractured. A combination of overload microvoids, which occupy most of the surface, and IG regions is evident. This observation is similar to that for the reference samples. Metallography did not reveal any abnormal features in this case too. The different behavior of samples H3 and H4, in comparison to samples H1 and H2, may be related to the significantly different cathode efficiencies that are involved in these two electrodeposition processes. While the cathode efficiency in hard chromium electrodeposition is only about 14%, the cathode efficiency in cadmium electrodeposition may approach 95%. This means that much more hydrogen is evolved near the surface of the chromium-coated metal, thus increasing the likelihood of HE.

Cadmium coating was applied also on steel of higher hardness (samples H5 and H6). In this case, the samples fractured already after 90 h of loading. Fig. 6 shows that the fracture surface in this case is still characterized by a combination of overload microvoids and IG regions. It should be noted that as the circumference of the sample is approached, the IG character becomes more dominant, although microvoid regions are still evident. Metallography showed no abnormal features. Comparison between Figs. 5 and 6 demonstrates the effect of hardness on the susceptibility to (or extent of) HE — the higher the hardness, the higher the susceptibility.

Sample SCC1 was tensile-tested under constant load while being exposed to solution of 3.5% NaCl; it failed after 800 h. Visual inspection revealed that the sample was covered with corrosion products. SEM inspection showed evidence of general corrosion, but not of SCC. In general, such behavior may result from not reaching the threshold plain-strain stress-intensity coefficient (K_{ISCC}) in this sample. Thus, no further analysis of this sample was carried out.

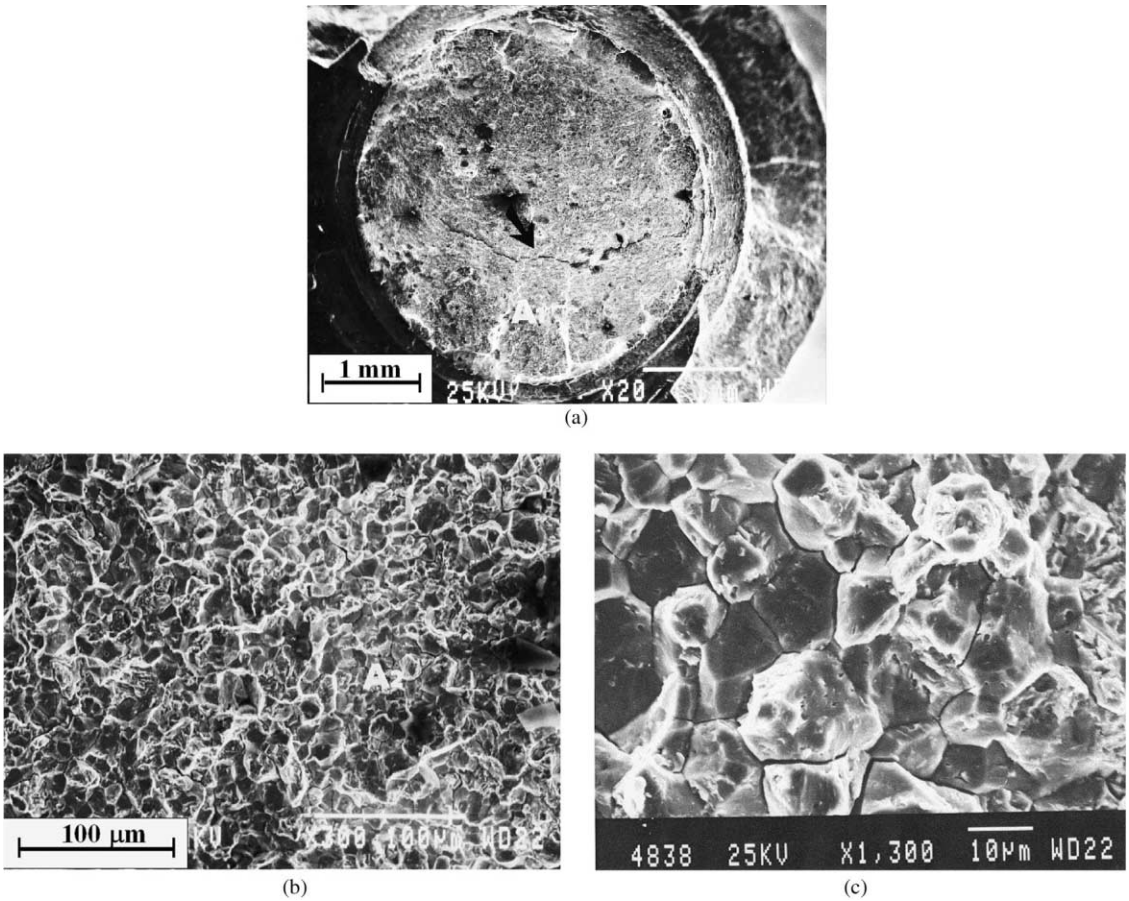

Fig. 4. SEM view of the fracture surface of a tensile V-notch sample made of AISI 4340 alloy steel (43–46 R_C) and electrodeposited with hard chromium, with no subsequent baking, after fracture by constant-load tensile test. (b) Higher magnification of region A_1 in (a). (c) Higher magnification of region A_2 in (b).

Cracking in both sample SCC2 and sample SCC3 was found to initiate after about 24 h of loading. Visual inspection showed that the cracks propagated in the tangential direction. After 72 h, the experiment was terminated, and the cracks opened (mechanically) for fractographic analysis. Visual inspection revealed much corrosion products on the surface of the samples. In addition, many secondary cracks were observed on the circumference of the samples, close to the fracture surface. Fig. 7 shows the typical fracture surface of these samples. Most of the surface is clearly IG, although some microvoid regions are evident as well. The grain facets exhibit an etched, dull appearance. In addition, cracking (most likely of the corrosion-product layer) is evident on some facets. Also evident is much secondary cracking within the samples, propagating from the fracture surface to the bulk. Finally, both crack branching and some significant separation of grains in vicinity to the crack are noticed.

Fig, 7(e) shows the metallographic cross-section that was prepared perpendicular to the fracture surface (the latter being marked by finger) of sample SCC3. A secondary, branched crack (marked by arrow) is noticed, propagating in parallel to the fracture surface. This observation is in accordance with the general characteristics of SCC, according to which the macroscopic path of cracks is always normal to the tensile

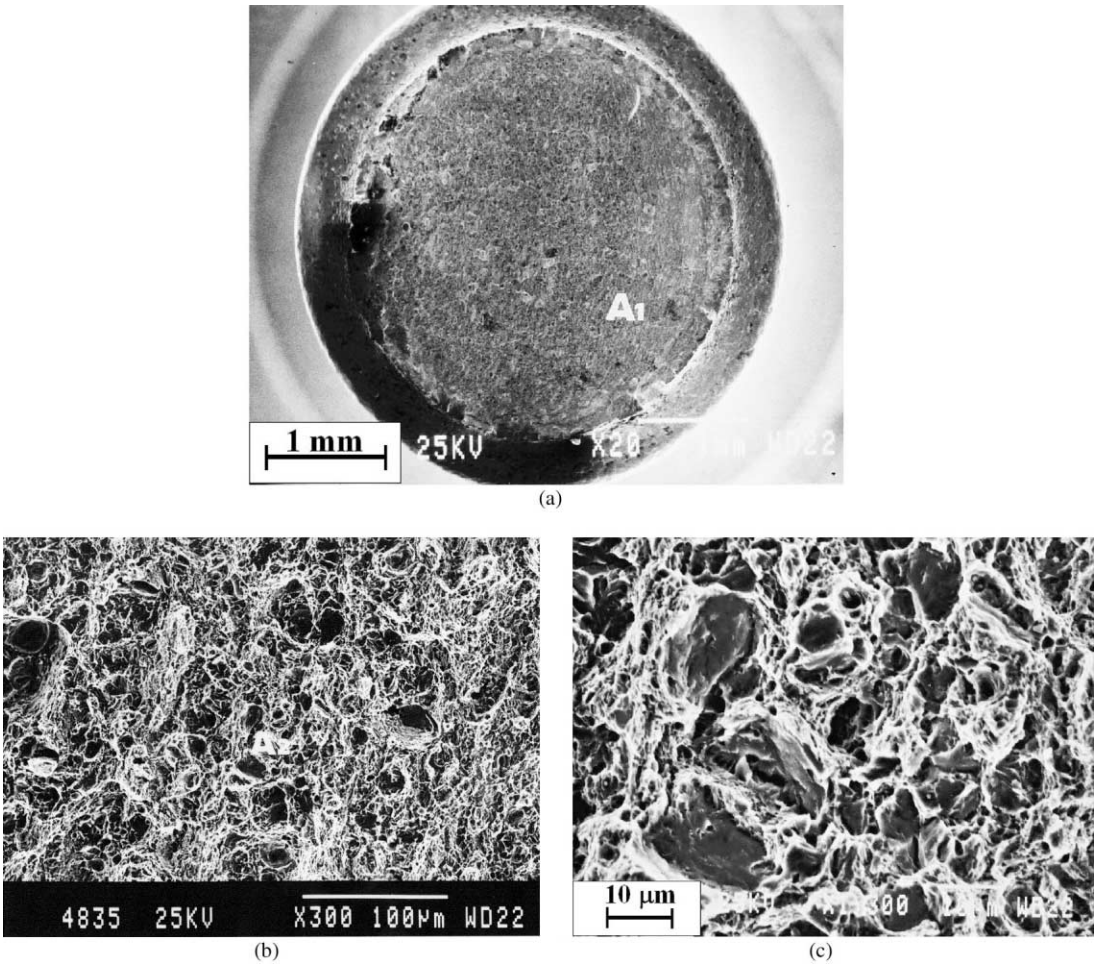

Fig. 5. SEM view of the fracture surface of a tensile V-notch sample made of AISI 4340 alloy steel (43–46 R_C) and electrodeposited with cadmium, with no subsequent baking, after fracture by constant-load tensile test. (b) Higher magnification of region A_1 in (a). (c) Higher magnification of region A_2 in (b).

component of stress. Comparing these results for samples SCC2 and SCC3 to the results for samples H1 to H6, the following conclusions may be drawn:

1. Much more secondary cracking occurs in the SCC samples compared to the H samples.
2. Although slightly dimpled, the grain facets in the H samples are relatively smooth and bright. In contrast, the grain facets in the SCC samples are considerably etched and have dull appearance.

Fig. 8 shows the typical fracture surface of sample TME1. The whole surface is characterized by a combination of microvoid and IG regions. It should be noted this pattern was found to be uniform across the whole fracture surface. Fig. 8(d) and (e) (LM) show the metallographic cross-section that was prepared perpendicular to the fracture surface (the latter being marked by finger). A crack (arrow) is seen to propagate from the notch region. The crack is oriented at about 40° relative to the fracture surface, and is about 0.1-mm long. No crack branching is evident. In addition, a thin dark layer, probably due to oxidation, can be seen on the crack walls. Similar results, including crack propagation from the notch region,

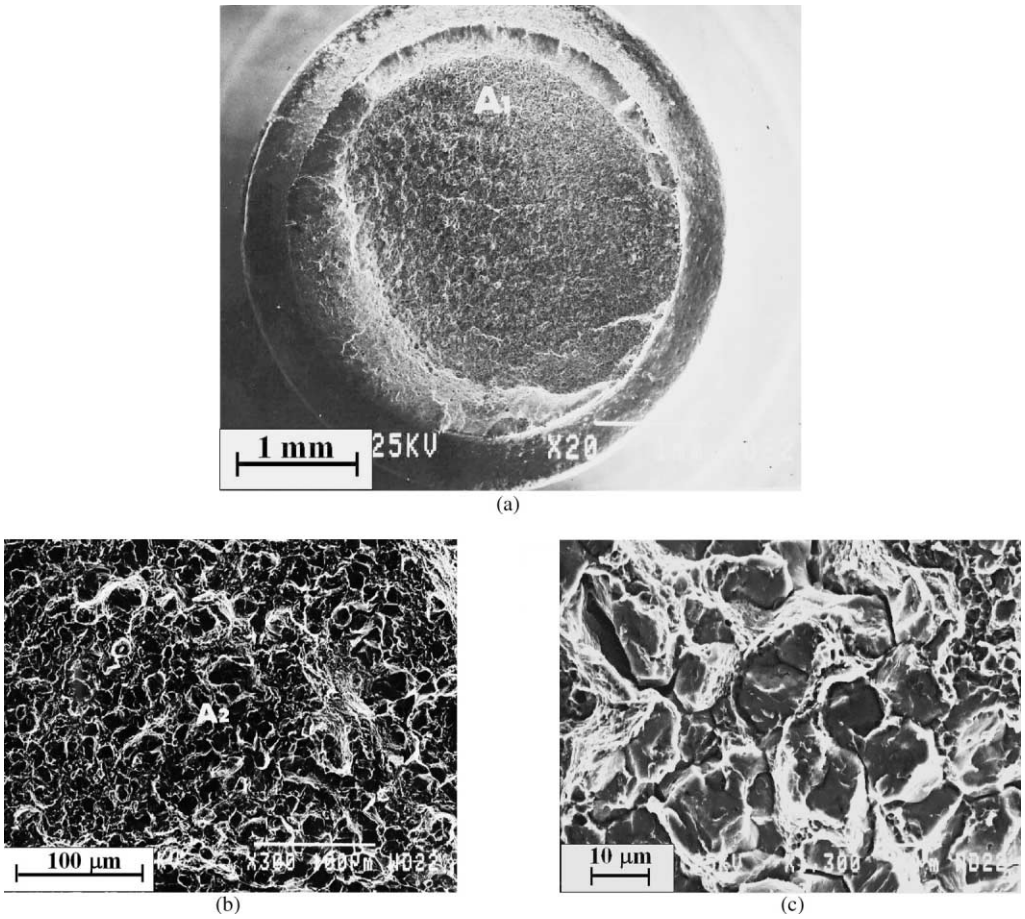

Fig. 6. SEM view of the fracture surface of a tensile V-notch sample made of AISI 4340 alloy steel (50–53 R_C) and electrodeposited with cadmium, with no subsequent baking, after fracture by constant-load tensile test. (b) Higher magnification of region A_1 in (a). (c) Higher magnification of region A_2 in (b).

were obtained for sample TME2. The characteristic fracture surface of sample TME3, which was austenitized at a higher temperature, is shown in Fig. 9. The IG pattern is much more dominant in this case, although some microvoid regions are still noticed. In addition, oxidation of both the fracture surface and the sample circumference is evident. The finding of oxidation on the fracture surface may indicate that the crack was formed during heat treatment (or, less probable in our case, already existed in the pre-treated sample). The dimples on grain facets may be related in this case to impurities that segregated to grain-boundaries prior to failure. Metallography did not reveal any abnormal features.

The fracture surface of sample TME4 that was austenitized at an even higher temperature was composed of IG regions, as well as of some regions that could not be defined because of excessive oxidation (Fig. 10). Again, this supports the formation of crack already during heat treatment. Metallography too showed that the sample was highly oxidized [Fig. 10(c)]. Therefore, another sample (TME5) was austenitized at the same temperature, but in vacuum. Visual inspection following impact test revealed a very bright fracture surface. The fracture surface was characterized by a distinct IG pattern (Fig. 11). No oxidation was observed in this case. Metallography supported the observation of a very distinct IG fracture path.

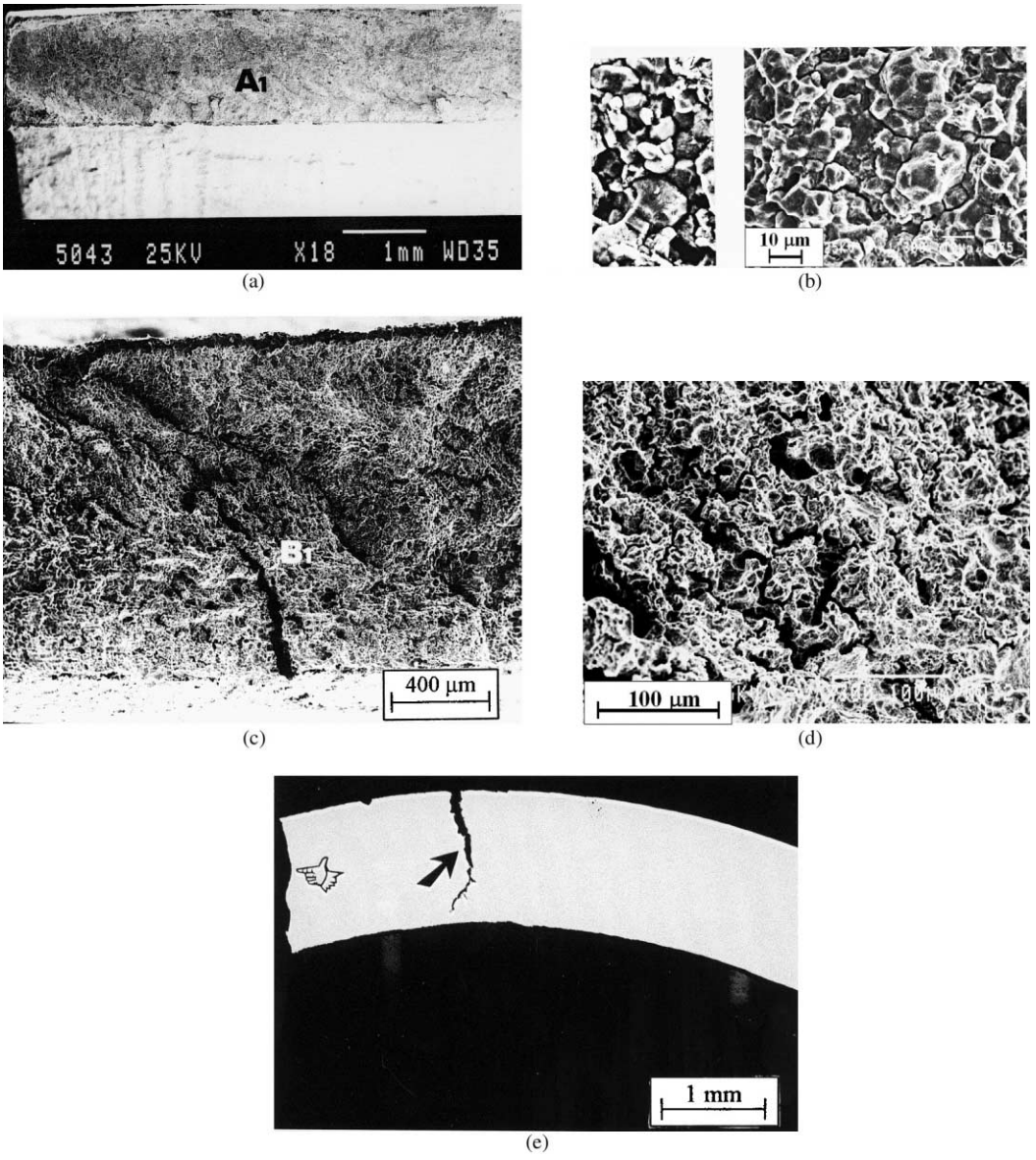

Fig. 7. SEM and LM view of the fracture surfaces of C-ring samples made of AISI 4340 alloy steel (43–46 R_C) cracked during alternate exposure to 3.5% solution. (a) and (b) were taken from sample SCC2 (Table 3). (c)–(e) were taken from sample SCC3. (b) Higher magnification of region A_1 in (a). (d) Higher magnification of region B_1 in (c). (e) Light microscopy view of a cross-section prepared perpendicular to the fracture surface (marked by finger).

Comparison between samples TME1, TME3 and TME4 shows that as the austenitization temperature is increased, the fracture surface becomes more IG. This behavior results from a synergistic effect of:

1. Increased dissolution of impurities at higher temperatures, which enhances their segregation to grain-boundaries.

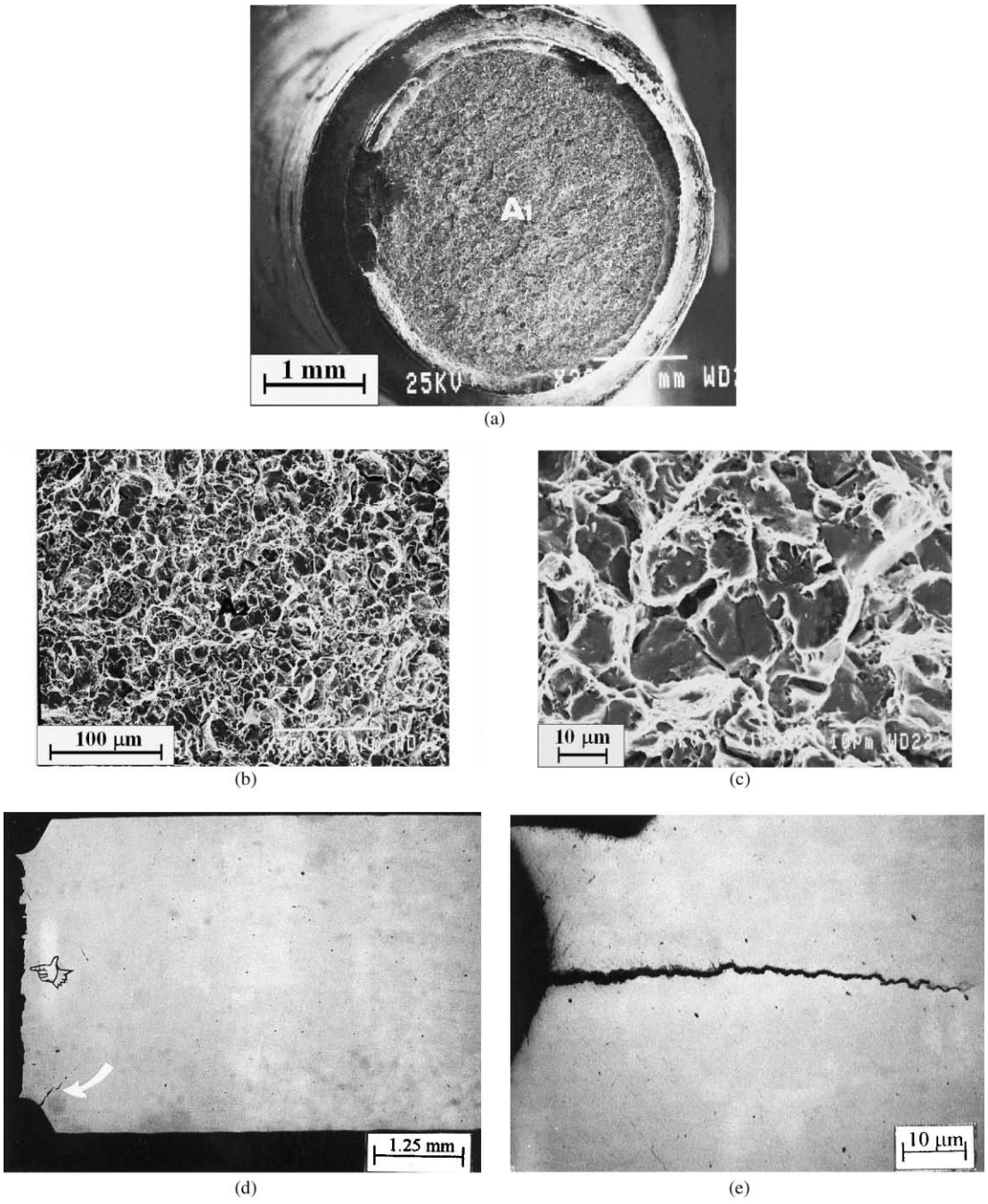

Fig. 8. SEM and LM view of the fracture surface of a tensile V-notch sample made of AISI 4340 alloy steel, austenitized at 850°C, oil-quenched, tempered at 350°C, and fractured by Charpy impact test. (b) Higher magnification of region A_1 in (a). (c) Higher magnification of region A_2 in (b). (d) Light microscopy view of a cross-section prepared perpendicular to the fracture surface (marked by finger). (e) Higher magnification of the crack seen in (d).

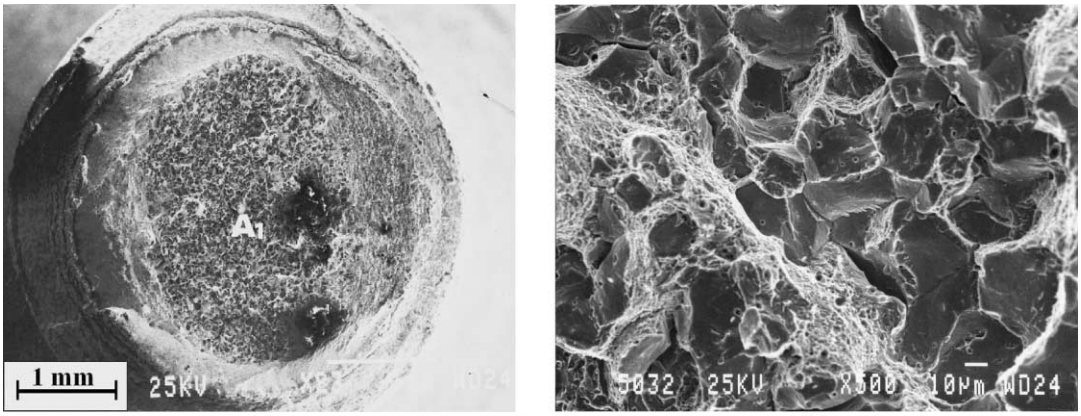

Fig. 9. SEM view of the fracture surface of a tensile V-notch sample made of AISI 4340 alloy steel, austenitized at 1000°C, oil-quenched, tempered at 350°C, and fractured by Charpy impact test. (b) Higher magnification of region A_1 in (a).

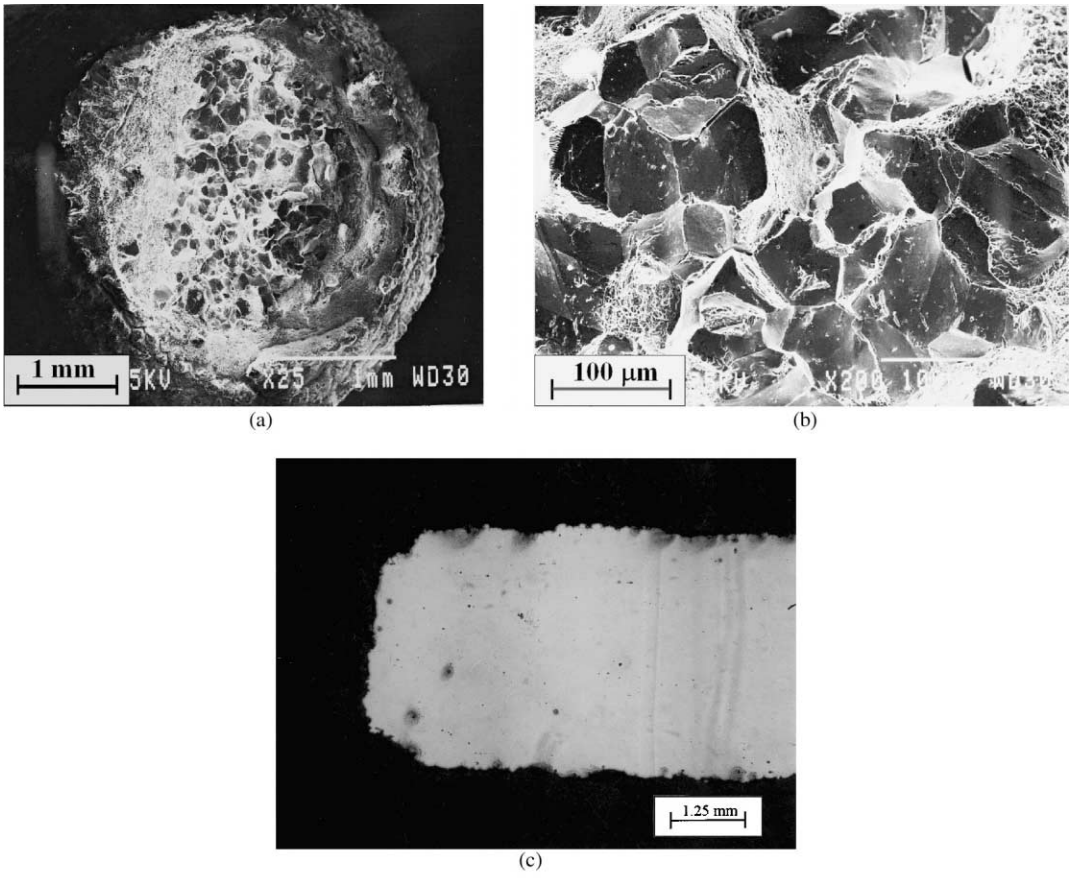

Fig. 10. SEM and LM view of the fracture surface of a tensile V-notch sample made of AISI 4340 alloy steel, austenitized at 1100°C, oil-quenched, tempered at 350°C, and fractured by Charpy impact test. (b) Higher magnification of region A_1 in (a). (c) Light microscopy view of a cross-section prepared perpendicular to the fracture surface.

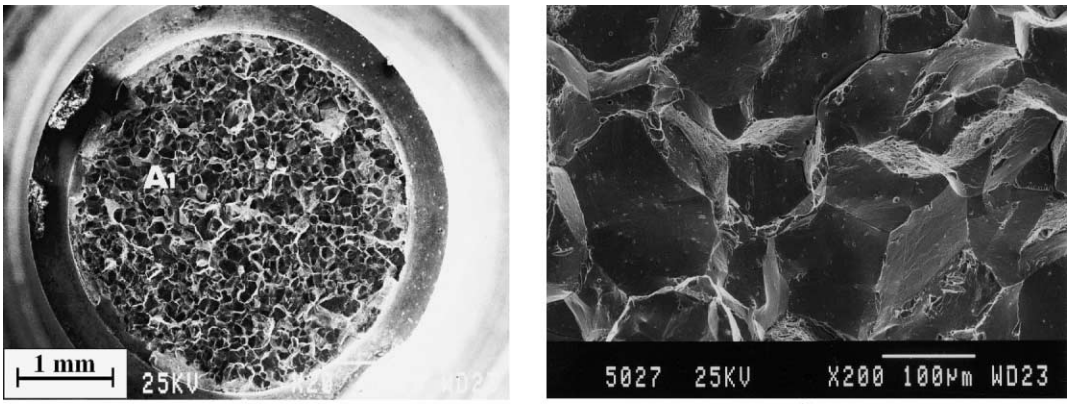

(a) (b)

Fig. 11. SEM view of the fracture surface of a tensile V-notch sample made of AISI 4340 alloy steel, austenitized in vacuum at 1000°C, oil-quenched, tempered at 350°C, and fractured by Charpy impact test. (b) Higher magnification of region A_1 in (a).

2. Increased austenite grain size at higher temperatures, leading to enrichment of grain-boundaries with impurities (see Section 1.1).

When increasing the austenitization temperature from 1000 to 1100°C, a significant increase in the level of oxidation is also evident. Compared to the samples embrittled by HE and SCC, the TME samples exhibit a more uniform fracture surface.

Neither microhardness testing nor X-ray diffraction was found to be useful in distinguishing between failures due to TME, HE, or SCC. The microhardness of all samples fell within the hardness range typical of the given heat treatment. No variation in microhardness as a function of distance from fracture surface was observed. Neither shift of peaks nor change in intensity in the X-ray diffractograms could be correlated unambiguously with a specific embrittling process. The spectra of all samples indicated the presence of α-Fe (*bcc* structure). In the case of sample TME5, reflections from γ-Fe (*fcc* structure) were also observed. However, these can be related to retained austenite in the heat-treated sample, rather than to an embrittlement effect. In this context, it should be noted that no other sample was austenitized similarly to sample TME5.

4. Conclusions

In this work, the characteristics of tempered martensite embrittlement (TME), hydrogen embrittlement (HE), and stress corrosion cracking (SCC) in high-strength steels were reviewed. In addition, samples made of AISI 4340 alloy steel were embrittled by controlled processes, fractured, and characterized using some common laboratory techniques. Results show that:

1. Assuming manufacturing/service conditions similar to those employed in this work, a careful fractographic examination may allow distinguishing between failures of AISI 4340 steel due to TME, HE, and SCC. The data presented in this paper may be used as reference for future failure analyses. In addition, knowledge of part manufacturing and service history is very helpful.
2. Microhardness testing and X-ray diffraction cannot be used as reliable tools for distinguishing between these three failure mechanisms, at least not under similar environmental conditions.
3. The susceptibility of AISI 4340 steel to HE in the absence of baking operation is much more significant for hard chromium electrodeposition than for cadmium electrodeposition.

4. An increased austenitization temperature leads to an increase in the portion of intergranular regions at the fracture surface of samples exposed to TME.

References

[1] Jones DA. Principles and prevention of corrosion. New York: Macmillan, 1992 (p. 234–89; 333–55).
[2] Lynch SP. Failures of structures and components by environmentally assisted cracking. Eng Failure Anal 1994;1(2):77–90.
[3] Briant CL, Banerji SK. Intergranular failure in steel: the role of grain-boundary composition. Int Met Rev 1978;23(4):164–99.
[4] Briant CL, Banerji SK. Intergranular fracture in ferrous alloys in nonaggressive environments. In: Briant CL, Banerji SK, editors. Treatise on materials science and technology, vol. 25. New York: Academic Press, 1983. p. 21–58.
[5] Hertzberg RW. Deformation and fracture mechanics of engineering materials. 4th ed. New York: John Wiley & Sons, 1996. p. 460–4; 485–520.
[6] Nelson HG. Hydrogen embrittlement. In: Briant CL, Banerji SK, editors. Treatise on materials science and technology, vol. 25. New York: Academic Press, 1983. p. 275–359.
[7] Tien JK, Thompson AW, Bernstein IM, Richards RJ. Hydrogen transport by dislocations. Metall Trans A 1976;7A(6):821–9.
[8] Stroh AN. A theory of the fracture of metals. Adv Phys 1957;6(24):418–65.
[9] Beachem CD. A new model for hydrogen-assisted cracking (hydrogen "embrittlement"). Metall Trans 1972;3(2):437–51.
[10] Shih DS, Robertson IM, Birnbaum HK. Hydrogen embrittlement of alpha titanium: in situ TEM studies. Acta Metall 1988;36(1):111–24.
[11] Birnbaum HK. Mechanisms of hydrogen related fracture of metals. In: Moody NR, Thompson AW, editors. Proceedings of the Fourth International Conference on the Effect of Hydrogen on the Behavior of Materials. Wyoming, 1990: Warrendale: TMS, 1989. p. 639–60.
[12] Beghini M, Benamati G, Bertini L. Hydrogen embrittlement characterization by disk pressure tests: test analysis and application to high chromium martensitic steels. J Eng Mater Technol 1996;118(2):179–85.
[13] Jung P. Compositional variation of hydrogen permeability in ferritic alloys and steels. J Nucl Mater 1996;238(2-3):189–97.
[14] Shiraga T, Ishiguro M, Yamashita E, Mizoguchi S. Effects of Ni, Si and Cu on the properties of steel bars for prestressed concrete. NKK Tech Rev 1996;75:11–18.
[15] Liou HY, Shieh RI, Wei FI, Wang SC. Roles of microalloying elements in hydrogen induced cracking resistant property of HSLA steels. Corrosion 1993;49(5):389–98.
[16] Riecke E, Johnen B, Liesegang H, Thoms A, Reynders B, Grabke HJ. Effects of Mo, V, Nb, Ti, Zr and their carbides on the corrosion and hydrogen uptake of iron in sulfuric acid. Werkst Korros 1988;39(11):525–33.
[17] Buckley P, Placzankis B, Lowder L, Brown IG, Brown R. Noble metal implantation to reduce hydrogen embrittlement in steels. Surf Coat Technol 1991;49(1–3):500–3.
[18] Wilson AD. Clean steel technology — fundamental to the development of high performance steels. In: Mahaney J.K. Jr., editor. Advances in the production and use of steel with improved internal cleanliness. West Conshohocken: ASTM, 1999: ASTM STP, 1361. p. 73–88.
[19] Latanision RM, Opperhauser Jr H. The intergranular embrittlement of nickel by hydrogen: the effect of grain boundary segregation. Metall Trans A 1974;5(2):483–92.
[20] Latanision RM, Opperhauser Jr H. Further observations on the effect of grain boundary segregation in the hydrogen embrittlement of nickel. Metall Trans A 1975;6(1):233–4.
[21] Eberhart ME, Latanision RM, Johnson KH. The chemistry of fracture: a basis for analysis. Acta Metall 1985;33(10):1769–83.
[22] Eberhart ME, Johnson KH, Latanision RM. A molecular orbital model of intergranular embrittlement. Acta Metall 1984;32(6):955–9.
[23] Eberhart ME, Latanision RM. The electrochemistry and solid state chemistry of intergranular hydrogen embrittlement. In: Jones RH, Gerberich WW, editors. Proceedings of the Symposium on Modeling Environmental Effects on Crack Growth Processes. Toronto, 1986: Warrendale: TMS, 1985. p. 125–36.
[24] Vehovar L. Hydrogen embrittlement of microalloyed structural steels. Werkst Korros 1994;45(6):349–54.
[25] Alvarez Laso J.A. and Gutiérrez-Solana F. Hydrogen induced cracking processes in structural microalloyed steels: characterization and modelling. In: Rodriguez-Ibabe, Gutiérrez I, López B, editors. Proceedings of the International Conference on Microalloying in Steels, Basque Country, 1998. Mater Sci Forum, vol. 284–286. Switzerland: Trans. Tech. Publ., 1998. p. 303–10.
[26] Toribio J, Lancha AM. Effect of cold drawing on susceptibility to hydrogen embrittlement of prestressing steel. Mater Struct 1993;26:30–7.
[27] Jung P. Hydrogen inventory and embrittlement in low activation steels. J Nucl Mater 1998;258-263:124–9.
[28] Jones RH, Ricker RE. Stress-corrosion cracking. In: Metals handbook, vol. 13. 9th ed. Ohio: ASM International, 1987. p. 145–63.

[29] Parkins RN. Stress corrosion cracking. In: Gangloff RP, Ives MB, editors. Proceedings of the First International Conference on Environment-Induced Cracking of Metals, Wisconsin. Houston, 1990: NACE, 1988. p. 1–19.
[30] Staehle RW, Hochmann J, McCright RD, Slater JE, editors. Proceedings of the Conference on Stress Corrosion Cracking and Hydrogen Embrittlement of Iron Base Alloys, Unieux-Firminy, 1973. Houston: NACE, 1977.
[31] AMS 6415. Steel bar forging and tubing (0.8Cr 1.8Ni 0.25Mo 0.38-0.43C (SAE 4340)). SAE Standard, January 1999.
[32] P.S. 01.9001. Heat treatment of carbon and low alloy steels other than case hardening and tool steels. Israel Aircraft Industry, 1984.
[33] ASTM F 519. Standard test method for mechanical hydrogen embrittlement evaluation of plating processes and service environments. West Conshohocken: ASTM, 1993.
[34] QQ-C-320. Chromium plating (electrodeposited). Federal Specification, 1987.
[35] QQ-P-416. Plating, cadmium (electrodeposited). Federal Specification, May 1995.
[36] ASTM E 8. Standard test methods for tension testing of metallic materials. West Conshohocken: ASTM, 1999.
[37] ASTM G 38. Standard practice for making and using C-ring stress-corrosion test specimens. West Conshohocken: ASTM, 1973.
[38] ASTM G 44. Standard practice for exposure of metals and alloys by alternate immersion in neutral 3.5% sodium chloride solution. West Conshohocken: ASTM, 1994.